Optimizing LGS WFS Pixel Processing in the Context of Evolving Turbulence and Sodium Profile

Lianqi Wang*and Brent Ellerbroek

Thirty Meter Telescope Project, 1111 S. Arroyo Pkwy, Suite 200, Pasadena, CA, 91105, USA

The time evolution of the sodium profile greatly impact the accuracy of laser guide star (LGS) wavefront sensor (WFS) measurements, for either the traditional thresholded center of gravity or the more advanced constraint matched filter/correlation algorithms. As a result, circularly symmetric wavefront aberrations will be induced in the adaptive optics (AO) corrected science wavefront for center launch LGS. In this paper, we describe our scheme to mitigate this issue by updating pixel processing parameters and employing a truth WFS during LGS AO operation. We also present simulation results using the sodium profiles measured by the UBC lidar. In addition, the time evolution of the turbulence profile will also have an impact on the pixel processing accuracy for the advanced algorithms, as well as the minimum variance wavefront reconstruction. We present simulation results showing how often we have to update the corresponding parameters to minimize the effect.

1. INTRODUCTION

Sodium laser guide star (LGS) Shack-Hartmann wavefront sensors (WFSs) suffer measurement uncertainty due to variations in the sodium layer.[1] The variation in the averaged range to the sodium layer causes focus measurement error (after reconstruction from gradients) that increases proportionally by the area of the telescope primary mirror and becomes unacceptable even at short time scales (~10 Hz) for extremely large telescopes (ELTs). The usual approach is to use natural guide stars WFS measurements to update the focus component of the LGS gradients reference vector at similar time scales. For AO systems that employ multiple laser guide star, past measurements[2] has suggested that there may also be significant differences in focus errors between these different laser beams. To mitigate this effect, we have adopted an novelty approach that applies an independent high pass filter (HPF) to the focus mode measurement of each LGS WFS, while simultaneously applying an complementary low pass filter (LPF) on the focus mode measurement of the low order NGS WFS. This removes the both the global and differential focus measurement error that are largely in the longer time scale. We still trust the focus measurement of LGS WFS in shorter time scale where the NGS WFS is not fast enough to provide measurement. The frequency split depends on the brightness of the NGS and the variation time scale of such focus measurement error.

In additional to moving up/down as a whole, the sodium layer also evolves in its vertical profile. This will cause additional measurement errors that depend on the separation between the sub-aperture and the laser launch telescope (LLT). For central launch adaptive optics (AO) systems, like the Thirty Meter Telescope (TMT) Narrow Field InfraRed Adaptive Optics System (NFIRAOS), the measurement error only contains radially symmetric modes. A moderately higher order but low speed natural wavefront sensor is consequently necessary to remove such radially symmetric errors. Such a WFS is conveniently named as a truth wavefront sensor (TWFS). In this report, we show that a pyramid WFS is welled suited for TWFS by presenting physical optics simulation results with different guide star brightness.

The sodium profile variation and turbulence profile variation also causes gain variations in the LGS WFS measurement algorithm, which, if not corrected, causes the non-common-path aberration (NCPA) calibration vectors to be incorrectly applied. This is usually corrected by dithering the laser beam at certain pattern using fast steering mirrors (FSMs) and matching the measured pattern to the actual pattern caused by the FSM. For NFIRAOS, a noise optimal algorithm with extend dynamic range called constrained matched filter is used instead of the usual (thresholded) center of gravity for pixel processing. A new matched filter is generated every few seconds to remove the gain error.

Previous bench test[3] has studied the effectiveness of updating matched filter together with a Shack-Hartmann WFS to concur the effect of sodium profile evolution. However, that work was based upon a scaled down version of NFIRAOS into classic single conjugate AO mode due to hardware and software limits. It also failed to account for the laser time-of-flight propagation delay between the FSM in the LLT and the LGS WFS, which will incur systematic gain error in the

*Send correspondence to Lianqi Wang (lianqiw@tmt.org)

real system. In addition, we show that in AO systems employing multiple laser beams, additional complexities arise in the matched filter update that need to be taken care of.

The following sections are organized as follows. Section 2 presents the parameters of the TMT AO system NFIRAOS which our modeling is based upon and our simulation parameters. Section 3 describes our estimation of the spatial and temporal power spectrum density (PSD) of measurement errors in focus and higher order radially symmetric modes. Section 4 describes the gain update of CoG or matched filter by dithering the laser beams and optimal update rate as determined by simulation. Section 5 describes the wavefront gradient reference vector update using TWFS measurements as well as subaperture reference image drift control in matched filter updating process. Section 6 presents the end to end simulation results and trade studies with time evolving sodium and turbulence profiles. Section **??** presents the conclusion.

2. NFIRAOS

The TMT NFIRAOS[4] is an order 60x60 MCAO system with two deformable mirrors (DMs) conjugated to ranges of zero and 11.2 km. An asterism of six sodium LGS at 90 km altitude arranged in a pentagon of 35" radius plus on axis are sensed by LGS Shack-Hartmann WFS. Up to three NGS are picked off by low order on-instrument wavefront sensors sensing in the infrared. The imaging instrument can optionally provide four on-detector-guide-windows for fast tip/tilt sensing and/or low speed flexure compensation. One pyramid WFS in NFIRAOS is used to provide truth wavefront sensing in LGS AO mode and high order wavefront sensing in classic NGS AO mode. The pyramid WFS has a band pass of 0.61-0.785μm with a nominal order of 96x96 and optional power of 2 binning factors (up to 16).

Our simulations are based upon the full scale model of NFIRAOS, with 7 256x256 meter turbulence layers sampled at 1/64 meter. Each screen is further multiplied by a matching scaling map generated from a spatial PSD to simulate the variation of seeing as measured (and extrapolated) from DIMM/MASS measurement data[5]. The turbulence profile used in simulation is listed in Table 1. A realization of design, polishing, and alignment error of telescope, AO and instrument optics are included . The DM flat and WFS calibration reference vector are computed based upon ray tracing results of these optics.

A total of eight sets of continuously evolving sodium layer profiles as measured on 20100731 by UBC lidar are binned down to 200 meter spatial and 1 second temporal sampling. The profiles are played at the same speed during simulation, with linear interpolation in between sampling points. The LGS focus error is slowly fixed by a focus mechanism (trombone) shared by all six LGS with an update rate of 0.3 seconds. The trombone is set to null the LGS WFS focus error in the beginning of simulation to simulate the LGS focus acquisition step. The LGS WFS pixel processing starts with center of gravity and switches to matched filter when the first estimate is available and then updates the matched filter regularly (nominally every 10 seconds).

The nominal signal level per frame for each fully illuminated LGS subaperture is 900 PDE. The read out noise of LGS WFS is 3e. The pyramid WFS detector has 1e read out noise. Slodar[6] is used during the simulation to estimate the turbulence profile and update the tomography weighting.[7]

Our simulation software, MAOS,[8] accelerates the simulation by simultaneously utilizing multiple graphical processing units (GPUs) for the most demanding computations and consequently enables high fidelity end to end simulations of those back ground processes that typically require minutes to hours of AO time. For example, with 8 Nvidia GTX 580 GPUs, we can simulate the full NFIRAOS with a wall clock to AO clock ratio of 20:1.

3. SODIUM PROFILE EVOLUTION

The sodium layer and turbulence profile evolution can introduce a mismatch between the matched filter used for pixel processing and the actual subaperture images for LGS WFS. This mismatch results in gradient gain error (difference of the response curve from unity) and offset error (nonzero gradient measurement with a flat wavefront). The gradient gain error has the effect of scaling the non-common-path-aberration (NCPA) gradient offsets, much like a centroid gain estimation error in an NGS WFS. For central launch LGS, the gradient gain and offset error is only along the radial direction (where elongation happens) and is a function of the distance from the LLT. After wavefront reconstruction, this gradient offset error results in erroneous radially symmetric modes being apply to the DM and consequently degrades science performance. The

Altitude (km)	Layer Weighting (r_0=0.186m)	wind speed (m/s)
0	0.4557	5.6
0.5	0.1295	5.8
1	0.0442	6.3
2	0.0506	7.6
4	0.1167	13.3
8	0.0926	19.1
16	0.1107	12.1

Table 1: C_n^2 profile models for the Mauna Kea 13N site. TMT has no direct measurement of the outer scale. We use a conservative value of 30 m.[9]

matched filter update process, through dithering the subaperture images using a fast steering mirror, corrects the gradient gain error, while in the mean time a truth WFS (TWFS) observing a natural guide star is used to apply reference vector to the LGS WFS to remove the gradient offset error [See Sections 4 and 5].

To determine the required rate to correct focus and higher order radially symmetric modes, we computed the PSD of these modes in the LGS WFS measurements. The eight set of sodium profiles described in Section 2 were used. For each sodium profile, we computed the time averaged short exposure subaperture images using the optical transfer function (OTF) method described in a previous paper.[10] Then we computed the gradients using two pixel processing algorithms. The first algorithm was constrained matched filter (abbreviated as matched filter [MF] hereafter). In this case, the first profile was used to build the matched filter and calculate gradients on subaperture images (time averaged short exposure) build with other sodium profiles in the same set. For tCoG, gradients were computed on subaperture images of each sodium profile independently. Focus and the spherical mode (ignoring higher order radially symmetric modes as they are significantly smaller) are then projected from the gradients.

PSDs of the focus and spherical measurement errors are then computed for each set of sodium profiles (1000 seconds long) using FFT method and averaged over the eight set of profiles. Figure 1 shows the results. In the top panel, the solid lines show the PSD of focus error computed from matched filter and CoG. Both agree fairly well with the power law $30f^{-1.9}$m^2/Hz (4 nm WFE per meter of focus for 30 meter telescope) previously reported.[2] The colored dashed lines show the PSD of spherical error from matched filter and CoG. The fit to power law of the average of both results, $2.25f^{-1.72}$nm^2/Hz, is shown in the black dashed curve. In the bottom panel, the integration of the PSD is shown. Based on this results, to control the spherical aberration errors to within 10 nm (considering servo lag along) requires a bandwidth of TWFS to be at least 0.01 Hz.

Based on these temporal PSDs, we can compute the corresponding spatial PSDs and structure function assuming frozen flow of the sodium layer. Then we can estimate the difference of these modes between different LGS WFS. A spatial PSD of

$$\Phi(k) = ak^{-n} \tag{1}$$

can be converted to temporal PSD by assuming isotropic frozen flow:

$$\Phi(f) = B(\frac{1}{2}, \frac{n-1}{2}) a f^{-n+1} v^{n-2} \tag{2}$$

where v is the wind speed of frozen flow (we use 34.4m/s for sodium layer) and B is the beta function.

Let us consider the focus error temporal PSD first. From $\Phi_F(f) = 30f^{-1.9}$, we have $n = 2.9$. The spatial PSD will be$\Phi_F(k) = 14.5333v^{-0.9}k^{-2.9} = 0.6k^{-2.9}$nm^2/(1/m). The covariance function is simply the FFT of the spatial PSD:$B_F(\mathbf{r}) = \int \Phi_F(\mathbf{k}) \exp[-2\pi i \mathbf{r} \cdot \mathbf{k}] d\mathbf{k}$, and the structure function is $D_F(\mathbf{r}) = 2[B_F(\mathbf{0}) - B_F(\mathbf{r})]$. The NFIRAOS LGS asterism, is separated at about 70 arcsec, which is 30 meter at 90km. At this separation, the RMS difference of focus between different LGS WFS is 171 nm. If not taken care of properly, this difference will propagate through wavefront

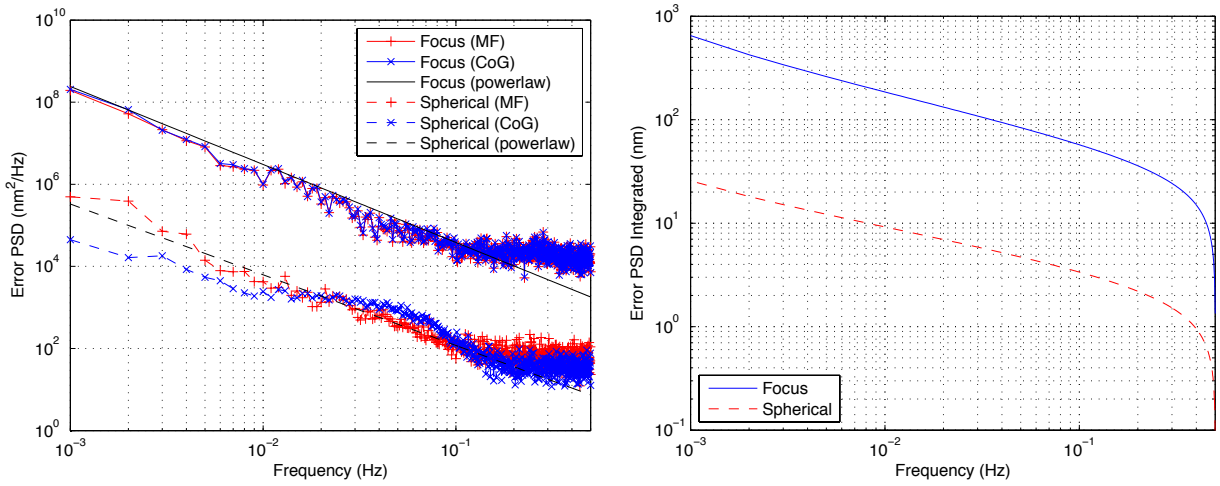

(a) PSD of focus and spherical aberration in LGS WFS measurements due to sodium profile evolution.

(b) Cumulative integration of the PSD (power law) from high frequency.

Figure 1: PSD of focus and spherical measurement error

tomography to non-focus modes that are not correctable by a low order NGS WFS that only measures focus. Our novel solution to this problem is to apply a HPF to the focus mode in each LGS WFS measurement, which removes a majority of the focus measurement error due to sodium profile evolution. A complementary low pass filter is simultaneously applied to the focus mode in the low order OIWFS measurements, which controls the low frequency focus error induced by the telescope optics or turbulence. The cross over frequency of the high/low pass filter can be further tuned based on the low order NGS sampling frequency.

For the spherical aberration WFE PSD, $\Phi_s(f) = 2.25 f^{-1.72}\text{nm}^2/\text{Hz}$. Converting to the spatial domain we have $\Phi_s(k) = 1.0244 v^{-0.72} k^{-2.72} = 0.08 k^{-2.72}\text{nm}^2/(1/\text{m})$. At a separation of 30m, the RMS difference of spherical aberration between different LGS WFS is about 7.5 nm. This difference will propagate through wavefront tomography to modes that are not correctable by a single TWFS. We can probably live with such a small error. Future simultaneous measurements of the sodium layer profile in several directions would be helpful in estimating this term. If proven necessary, we can apply a similar HPF on the spherical mode of each LGS WFS measurement like for the focus mode.

4. THE DITHERING PROCESS TO UPDATE MATCHED FILTER

4.1 Uplink Servo Analysis

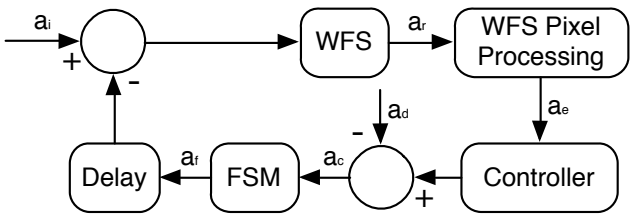

Figure 2: LGS beam uplink control

Figure 2 shows the block diagram for the LGS control servo to stabilize the laser pointing and injecting of dither signal. The delay box takes into account the RTC computation delay and laser beam time-of-flight propagation from laser launch telescope (LLT) up toward the sodium layer and back to the telescope. The variables are defined as follows:

- a_i: Subaperture image motion due to up and downlink turbulence and telescope wind shake or vibration.
- a_r: Averaged subaperture image motion during WFS exposure.
- a_e: Estimated subaperture motion by WFS pixel processing algorithm.
- a_d: Dithering signal.
- a_c: Uplink Fast Steering Mirror (FSM) tip/tilt command.
- a_f: Actual FSM tip/tilt position as measured by in situ sensor.

In Laplace domain, these variables satisfy the following equations:

$$\begin{aligned}
\hat{a}_r &= H_{wfs}\hat{a}_i - H_{wfs}H_D\hat{a}_f && (3)\\
\hat{a}_e &= g\hat{a}_r && (4)\\
\hat{a}_c &= \frac{1}{H_D H_{fsm}}\frac{H_{ol}\hat{a}_i}{1+H_{ol}} - \frac{\hat{a}_d}{1+H_{ol}} && (5)\\
\hat{a}_f &= H_{fsm}\hat{a}_c && (6)
\end{aligned}$$

where H_{wfs} is the transfer function of the WFS, H_D is the transfer function due to propagation delay, H_{fsm} is the transfer function of the FSM, g is the gain error of the pixel processing algorithm, H_{ol} is the end-to-end open loop transfer function.

4.2 The Dithering Process

Let the WFS sampling period be T, the time-of-flight propagation delay plus RTC computation delay be $\Delta_c T$, and the image motion (tip/tilt of wavefront) be represented by the real and imaginary component of a complex number. The dithering signal is chosen to be a discrete command that jumps between the four corners of a diamond:

$$a_d(t) = A_d \exp\left[\frac{i\pi}{2}\text{floor}\left(\frac{t}{T}\right)\right].$$

Let the servo phase and amplitude effect of the transfer function $H_{fsm}/(1+H_{ol})$ be ϕ_d and α, we have

$$\begin{aligned}
a_f(t) &= -\alpha a_d(t)\exp\left(-i\phi_d\right) + n_1\\
&= -\alpha A_d \exp\left[\frac{i\pi}{2}\text{floor}\left(\frac{t}{T}\right) - i\phi_d\right] + n_1.
\end{aligned}$$

where n_1 (and various n in the following equations) represent the effects of turbulence and photon noise. The averaged WFS subaperture image motion at time step k (from $(k-1)T$ to kT) is

$$\begin{aligned}
a_r[k] &= -\int_{(k-1)T}^{kT} a_f(t-\Delta_c T) + n_2\\
&= \frac{1}{T}\int_{(k-1)T}^{kT} \alpha A_d \exp\left[\frac{i\pi}{2}\text{floor}\left(\frac{t}{T}-\Delta_c\right) - i\phi_d\right] + n_3
\end{aligned}$$

There exists a factor $\beta = \Delta_c + 1 + \text{floor}(-\Delta_c)$. such that $\text{floor}\left(\frac{t}{T}-\Delta_c\right) =$

$$\begin{cases}
(k-1) + \text{floor}(-\Delta_c) & (k-1)T < t < (k-1+\beta)T\\
k + \text{floor}(-\Delta_c) & (k-1+\beta)T \le t \le kT
\end{cases}$$

We then have

$$\begin{aligned} a_r[k] &= \alpha A_d \exp\left[\frac{i\pi}{2}\left((k-1)+\text{floor}(-\Delta_c)\right)-i\phi_d\right] \\ &\quad \cdot\left(\beta+(1-\beta)\exp\left[\frac{i\pi}{2}\right]\right)+n_3. \end{aligned} \tag{7}$$

For convenient analysis, we can define an alternative variable $b[k]$ that has same phase as $a_r[k]$ but with unit magnitude:

$$\begin{aligned} b[k] &= \frac{\left(\beta+(1-\beta)\exp\left[\frac{i\pi}{2}\right]\right)}{\left(\beta^2+(1-\beta)^2\right)} \\ &\quad \cdot\exp\left[\frac{i\pi}{2}\left((k-1)+\text{floor}\left(-\Delta_c\right)\right)-i\phi_d\right]+n_4. \end{aligned}$$

4.3 Estimate servo delay and dithering amplitude

A delay locked loop can be used to estimate the phase ϕ_d of $H_{fsm}/(1+H_{ol})$ by locking the phase of estimated $b[k]$ to the measured image motion $a_e[k]$. The phase difference between the estimated $b[k]$ and $a_e[k]$ can be approximated by their normalized cross product:

$$\theta_{dll} \approx \left\langle \frac{1}{A_d}(b^x[k]a_e^y[k]-b^y[k]a_e^x[k])\right\rangle_k .$$

A loop with gain of g_{dll} can be used to update the estimate of ϕ_d after averaging over a number of WFS frames:

$$\phi_d = \phi_d + g_{dll}\theta_{dll}$$

The amplitude of FSM position a_f, and therefore α can be computed by correlating a_f with the conjugate of a sinusoidal sequence that has the same frequency as the dithering signal but with arbitrary initial phase. In fact, for any sinusoidal signal a_f represented as,

$$a_f = A_f \exp[\frac{i\pi}{2}(k+\phi)]+n,$$

its amplitude can be determined by correlating it with $\exp[-\frac{i\pi k}{2}]$:

$$A_f = \left|\left\langle a_f \exp[-\frac{\pi i}{2}k]\right\rangle_k\right|.$$

Finally

$$\alpha = \frac{A_f}{A_d}$$

4.4 Updating Matched Filter

The constrained matched filter is a noise optimal algorithm used for the NFIRAOS LGS WFS gradient computation with superior performance than (thresholded) center of gravity. It needs to be updated periodically to account for the turbulence and/or sodium profile variations. Recall that in the matched filter formulation, we model the WFS subaperture image in each exposure using its Taylor expansion:

$$i[k] = i_0 + \frac{\partial i}{\partial \theta_x}a_r^x[k] + \frac{\partial i}{\partial \theta_y}a_r^y[k] + n_i \tag{8}$$

where i_0 is the subaperture image with zero image motion (approximated by the time averaged image), $\frac{\partial i}{\partial \theta_x}$, $\frac{\partial i}{\partial \theta_y}$ are the partial derivatives of the subaperture image i, $a_r^x[k]$ and $a_r^y[k]$ are tip and tilt component of WFS subaperture image motion, and n_i is effect of turbulence and photon noise.

The derivative of i in Eq 8 can be retrieved by correlating the WFS subaperture image with the tip and tilt components of $b[k]$ and average for a number of time steps:

We have

$$\begin{aligned} \langle i[k]b^x[k]\rangle_k &= \frac{\partial i}{\partial \theta_x}\langle a_r^x[k]b^x[k]\rangle_k = \frac{\partial i}{\partial \theta_x}\frac{\alpha A_d}{2} \\ \langle i[k]b^y[k]\rangle_k &= \frac{\partial i}{\partial \theta_y}\langle a_r^y[k]b^y[k]\rangle_k = \frac{\partial i}{\partial \theta_x}\frac{\alpha A_d}{2} \end{aligned}$$

Therefore,

$$\begin{aligned} \frac{\partial i}{\partial \theta_x} &= \frac{2}{\alpha A_d}\langle i[k]b^x[k]\rangle_k \\ \frac{\partial i}{\partial \theta_y} &= \frac{2}{\alpha A_d}\langle i[k]b^y[k]\rangle_k \end{aligned}$$

The rest of the matched filter computation follows the procedure outlined in a previous paper.[10]

4.5 Updating CoG Gain

To update the center of gravity algorithm, we just need to correct the gain error g in Eq 4 by correlating the x and y component of a_e with b:

$$\langle a_e^x[k]b^x[k]\rangle_k = g_{xx}\frac{\alpha A_d}{2} \tag{9}$$

$$\langle a_e^y[k]b^y[k]\rangle_k = g_{yy}\frac{\alpha A_d}{2} \tag{10}$$

Therefore,

$$g_{xx} = \frac{2}{\alpha A_d}\langle a_e^x[k]b^x[k]\rangle_k \tag{11}$$

$$g_{yy} = \frac{2}{\alpha A_d}\langle a_e^x[k]b^y[k]\rangle_k \tag{12}$$

5. LGS WFS REFERENCE VECTOR

The LGS WFS gradients are adjusted by subtracting a reference vector, denoted as R_k for LGS WFS number k, at every frame. It is composed of three components:

$$R_k = s_{ncpa} + S_F\text{LPF}\left[R_F s_{lgs}\right] + r_k. \tag{13}$$

Here s_{ncpa} is the reference vector for calibrating the NCPA. The LGS WFS gradient vector s_{lgs} is projected to focus mode by $R_F = S_F^\dagger$, low pass filtered, and then mapped back to LGS gradients by S_F. The vector r_k is adjusted by the matched filter and truth WFS update process to compensate for errors caused by turbulence and sodium profile evolutions.

The TWFS measurement is incorporated to the reference vector by an integrator

$$r_k = r_k - g_{twfs}S_R R_{twfs}s_{twfs} \tag{14}$$

where s_{twfs} is TWFS gradient vector, R_{twfs} reconstructs TWFS gradients on to radially symmetric modes and S_R maps the radial modes onto LGS gradients, and finally g_{twfs} is the integrator gain.

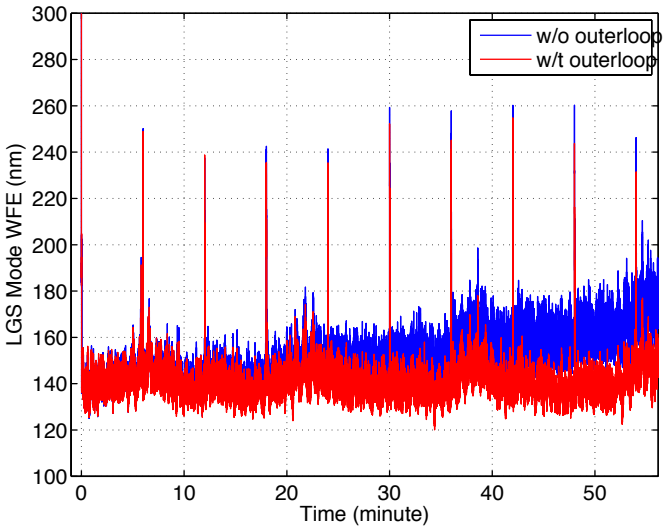

Figure 3: Compare 60 minute simulations with and without outer loop to control i_0 drift.

We discovered in simulations that simply relying on the TWFS to update the LGS WFS gradient offset vector, in parallel with the matched filter update of the pixel processing weights does not work in MCAO mode without further modifications. The reason is that each LGS WFS will accumulate the averaged subaperture image at a slightly different averaged location than dictated by the reference vector due to different uplink/downlink turbulence and sodium profile and measurement noise. When matched filter is updated, each LGS WFS will compute gradients with respect to this erroneous reference point and a systematic bias is introduced. Since each LGS WFS has different errors, the end result is a performance degradation that is not correctable by a single TWFS. This error will eventually drive the system unstable.

The solution to this problem is to estimate the difference between the gradients of the average subaperture image and the reference vector, and adjust the reference vector to account accordingly. Let G_{prev} and g_r represent the previous pixel processing algorithms/parameters and gradient reference vector before switching to the new matched filter, we adjust the reference vector by

$$r_k = r_k - G_{prev} i_0. \tag{15}$$

This enables smooth transitioning to the new matched filter without artificial disturbance to the loop. This also decouples the matched filter update and the TWFS update processes, which can now run at different rates. After this modification, simulations show that the update process work well without stability issues.

In addition, to prevent the matched filter from drifting away on longer time scales, we need to drive the CoG of the averaged subaperture image toward the NCPA reference vector using an outer-loop with relatively low gain (~0.1):

$$r_k = r_k - 0.1 \times (G_{cog} i_0 + r_k - g_{ncpa}) \tag{16}$$

where G_{cog} represent pixel processing using thresholded CoG, and g_{ncpa} is the current NCPA gradient reference vector.

Figure 3shows the comparison of two 60 minute simulations with and without this outer loop. The sodium profile evolution and TWFS output is sped up by 5 times to accelerate the transition. The spikes are due to abrupt changes in sodium profiles due to wrap around during simulation. The difference between the two curve as time goes by clearly shows the importance of the outer loop. Close examination shows that one cycle of TWFS output ($g_{twfs} = 1$) followed by one cycle of matched filter update (the two processes are inter-leaved) brings the performance back to normal after each disturbance.

6. SIMULATION RESULTS AND PARAMETER TRADEOFF

Simulations have been carried out to quantify the performance degradation of the AO system due to sodium profile evolution while compensated with TWFS and matched filter update. The simulation parameters are described in Section 2. The following one AO-minute simulations were carried out to determine the optimal parameter and the associated residual error:

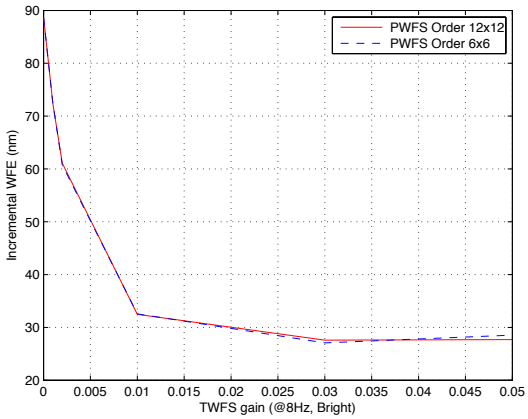

Figure 4: Compare gain of TWFS update.

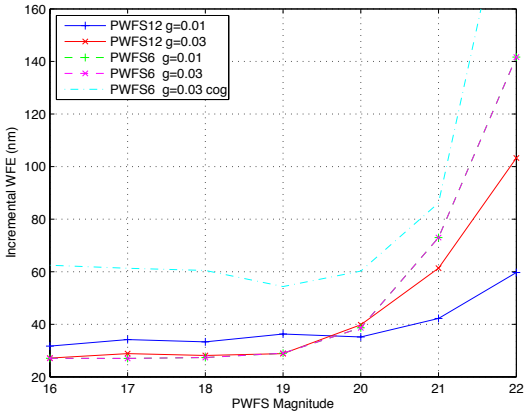

Figure 5: Performance of TWFS with PWFS at different magnitude.

1. Constant sodium profile, and theoretical matched filter built using the sodium profile.
2. Evolving sodium profile, with constant matched filter update rate and various TWFS correction bandwidth.
3. Evolving sodium profile, with constant TWFS correction bandwidth and various matched filter update rate.

The past studies[3] used Shack-Hartmann WFS as TWFS, keep the update gain g_{twfs} to 1 and varies the frame rate to vary the TWFS correction bandwidth. But for pyramid WFS used as TWFS, a faster frame rate is desirable so that the optical gain estimation of the PWFS has time to converge. We therefore set the frame rate of TWFS to 8 Hz (or lower when guide star brightness is too low) and vary the TWFS update gain g_{twfs}.

The results from case 1 are used as the baseline to compute incremental wavefront error (quadrature) of the other cases to quantify the penalty. Figure 4 shows such error versus the TWFS gain for PWFS binned to order 12x12 or 6x6. The optimal performance is achieved with order 6x6 at a gain of 0.03, which is roughly equivalent to 4 second frame rate with gain of 1.

Figure 5 shows the results for different PWFS brightness level, with different PWFS order and TWFS gain. The end to end throughput is about 35%. Mauna Kea 80 percentile sky background (R=19.1/arcsec^2) is assumed.[11] For bright PWFS guide stars, order 6x6 sensing with gain of 0.03 gives the optimal performance as expected. For dim PWFS guide stars, order 12x12 sensing with lowered gain of 0.01 gives the best performance. A guide star with R <= 20 can be used to limit the incremental WFE to below 35 nm. Results are also shown for the case that only 2σ-thresholded CoG is used with its gain updated by dithering. The performance is worst than matched filter by a large margin.

7. CONCLUSION

We presented methods for optimizing the LGS WFS measurement accuracy with evolving turbulence and sodium profiles. In particular, the LGS WFS pixel processing parameters and gradient reference vectors are adjusted periodically to correct the gain and offset error. The LGS WFS focus measurements are individually high pass filtered to remove focus measurement error induced by sodium altitude variation. The effectiveness of these methods are demonstrated by simulation results.

REFERENCES

[1] Herriot, G., Hickson, P., Ellerbroek, B., Véran, J.-P., She, C.-Y., Clare, R., and Looze, D., "Focus errors from tracking sodium layer altitude variations with laser guide star adaptive optics for the Thirty Meter Telescope," in [*Society of Photo-Optical Instrumentation Engineers (SPIE) Conference Series*], **6272** (July 2006).

[2] Pfrommer, T. and Hickson, P., "High-resolution lidar observations of mesospheric sodium and implications for adaptive optics," *JOSA A* **27**, A95–A105 (2010).

[3] Conan, R., Lardière, O., Herriot, G., Bradley, C., and Jackson, K., "Experimental assessment of the matched filter for laser guide star wavefront sensing," *Appl. Opt.* **48**, 1198–1211 (Feb 2009).

[4] Herriot, G., Andersen, D., Atwood, J., Boyer, C., Beauvillier, A., Byrnes, P., Conan, R., Ellerbroek, B., Fitzsimmons, J., Gilles, L., Hickson, P., Hill, A., Jackson, K., Lardière, O., Pazder, J., Pfrommer, T., Reshetov, V., Roberts, S., Véran, J.-P., Wang, L., and Wevers, I., "NFIRAOS: TMT's facility adaptive optics system," *SPIE Conference Series* **7736** (July 2010).

[5] Schöck, M., Els, S., Riddle, R., Skidmore, W., Travouillon, T., Blum, R., Bustos, E., Chanan, G., Djorgovski, S. G., Gillett, P., Gregory, B., Nelson, J., Otárola, A., Seguel, J., Vasquez, J., Walker, A., Walker, D., and Wang, L., "Thirty Meter Telescope Site Testing I: Overview," *PASP* **121**, 384–395 (Apr. 2009).

[6] Wang, L., Schöck, M., and Chanan, G., "Atmospheric turbulence profiling with slodar using multiple adaptive optics wavefront sensors," *Appl. Opt.* **47**, 1880–1892 (Apr 2008).

[7] Ellerbroek, B. L., "Efficient computation of minimum-variance wave-front reconstructors with sparse matrix techniques," *J. Opt. Soc. Am. A* **19**(9), 1803–1816 (2002).

[8] [*Computer simulations and real-time control of ELT AO systems using graphical processing units*], **8447** (2012).

[9] Abahamid, A., Vernin, J., Benkhaldoun, Z., Jabiri, A., Azouit, M., and Agabi, A., "Seeing, outer scale of optical turbulence, and coherence outer scale at different astronomical sites using instruments on meteorological balloons," *Astronomy and Astrophysics* **422**, 1123–1127 (Aug. 2004).

[10] Gilles, L. and Ellerbroek, B., "Shack-hartmann wavefront sensing with elongated sodium laser beacons: centroiding versus matched filtering," *Appl. Opt.* **45**(25), 6568–6576 (2006).

[11] "https://www.gemini.edu/sciops/telescopes-and-sites/observing-condition-constraints/optical-sky-background."